Hydro-elastic finite element model of a vocal fold replica

Nicolas Hermant, Xavier Pelorson, Paul Luizard, Franz Chouly, Fabrice Silva

Florence, Italy 12-16 July 2015
ICSV22
The 22nd International Congress on Sound and Vibration

HYDRO-ELASTIC FINITE ELEMENT MODEL OF A VOCAL FOLD REPLICA

Nicolas Hermant, Xavier Pelorson, Paul Luizard
GIPSA-lab UMR CNRS 5216, 11 rue des mathématiques, BP 46, 38402 Saint-Martin-D'Hères, France

Franz Chouly
LMB UMR CNRS 6623, Univ. Franche-Comté,25030 Besançon cedex, France

Fabrice Silva
LMA, CNRS, UPR 7051, Aix-Marseille Univ, Centrale Marseille, F-13402 Marseille cedex 20, France
email: silva@lma.cnrs-mrs.fr

Abstract

Experimental vocal fold replicas are currently used in speech production studies in order to validate simplified models on controllable devices. In addition to in-situ mechanical characterization, it is important to be able to understand their behavior when changing assembly properties or using parameters control to tune the folds, by developing a model able to predict their static and dynamic motions. This also enables to describe more complex vibration behaviors which could be harder to observe experimentally.
This paper first presents a hydro-elastic finite element model of a single vocal fold. Numerical results are discussed, along with a parametric analysis. Then this model is extended to take into account the effect of the water pressure on the inflation of the folds and on the resonance frequencies. A hyper-elastic calculation is first used to simulate the latex inflation. An updated Lagrangian approach processes it as a pre-stress term in a modal analysis calculation for the small amplitude vibrations of the hydro-elastic structure, which allows to model the water pressure influence on the mechanical resonances of the simulated replica.

1. Introduction

Voice is one of the most important communication vectors. Its degradation still leads to major difficulties within social interactions and voice disorders are to be considered as a public health issue. In support of clinical and rehabilitative practices, physical modeling brings a global understanding of phonatory organ pathologies, for which vocal folds are highly affected. In this modeling approach, experimental replicas have been developed notably since the work of Van Den Berg [1]. By reproducing the physical phenomena involved in speech production, these tools allow to validate simplified theoretical models, and a particular interest on the measurement and the control of vibrating structures has emerged lately.

The present study focuses on water-filled latex replicas as used in voice or brass instrument experiments, see e.g. Refs [2, 3]. The most recent design (see Fig. 1a) is made of a thin layer of latex

(thickness of 0.2 to 0.3 mm) surrounding a half-cylinder volume of water and its metallic support. The water pressure can be adjusted to get the proper stiffness and the metal parts are mobile to set the vocal folds closer as it is during the abduction phase. Then, the water and its latex envelope can vibrate as a result of a fluid-structure interaction with an airflow coming from artificial lungs. That coupling is not studied here.

The aim of this paper is to present a theory able to predict the influence of the water pressure on the resonance frequency of the structure. Such a problem also gained recently some interest in the domain of the deployable structures (also known as inflatables) used in spacecrafts (see, e.g., Ref [4]). A linear hydro-elastic model will be first described and exploited (Sec. 2), and then it will be adapted in the Lagrangian finite strain framework to introduce the prestress in the formulation, thus enabling the water-pressure dependency (Sec. 3).

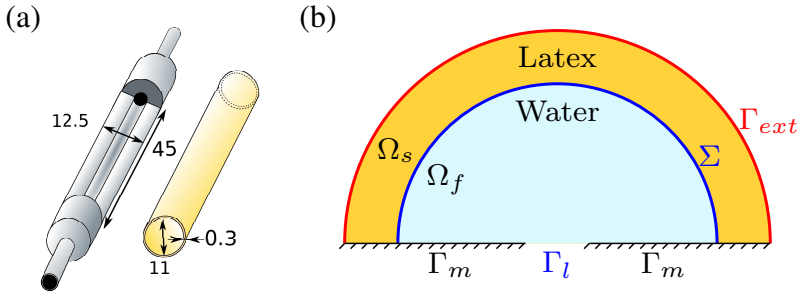

Figure 1: (a) Vocal fold components. (b) Boundaries, solid and fluid domains of the model.

2. Hydro-elastic modeling of the non-inflated replica

2.1 Modeling

The hydro-elastic linear modeling derives from Ref. [5], further step-by-step details are provided in Ref. [6] and an analysis of the spectral problem can be found in [7]. Fig. 1b illustrates the solid and the fluid domains and their respective nominal dimensions. The solid is first modeled as a deformable isotropic linear elastic material with density ρ_s under the small deformation hypothesis. It is submitted to the water pressure p on the boundary Σ, attached on Γ_m, all other volume forces or traction forces on Γ_{ext} being neglected, and harmonic solutions are sought (with convention $\exp j\omega t$). Denoting $\mathbf{u}_s$ the unknown displacement field and $\mathbf{v}$ the test function, a weak formulation of the elastodynamics implies the solid mass and stiffness bilinear operators $\mathcal{M}_s$ and $\mathcal{K}_s$:

$$\mathcal{M}_s(\mathbf{u}_s,\mathbf{v}) = \int_{\Omega_s} \rho_s \mathbf{u}_s \cdot \mathbf{v}\, d\Omega_s \quad \text{and} \quad \mathcal{K}_s(\mathbf{u}_s,\mathbf{v}) = \int_{\Omega_s} \sigma_s(\mathbf{u}_s) : \varepsilon(\mathbf{v})\, d\Omega_s \tag{1}$$

where σ and ε are the Cauchy stress and the small strain tensors, respectively.

The water is considered as an irrotational inviscid homogeneous Newtonian incompressible fluid with small displacements $\mathbf{u}_f$ and small pressure fluctuations p around the rest state. It is modeled using the Euler linearized equation which, as detailed in Ref. [6], allows to describe the fluid state with the fluid displacement potential φ, with $\mathbf{u}_f = \nabla\varphi$ and $p = \rho_f\omega^2\varphi$. This potential thus obeys to the Laplace's equation $\Delta\varphi = 0$ within the fluid domain, and vanishes on the wall. Boundary Γ_l is the inflation inlet where the static pressure can be imposed. Coupling between the solid and the fluid on the boundary Σ expresses through the complete transmission of the normal displacements and efforts:

$$\frac{\partial\varphi}{\partial\mathbf{n}} = \mathbf{u}_s \cdot \mathbf{n} \quad \text{and} \quad \sigma(\mathbf{u}_s)\cdot\mathbf{n} = \rho_f\omega^2\varphi\,\mathbf{n} \quad \text{on} \quad \Sigma. \tag{2}$$

Defining the fluid mass $\mathcal{M}_f$ and the coupling $\mathcal{C}_{fs}$ bilinear operators as

$$\mathcal{M}_f(\varphi,\psi) = \int_{\Omega_f} \rho_f \nabla\varphi\cdot\nabla\psi\, d\Omega_f \quad \text{and} \quad \mathcal{C}_{fs}(\mathbf{u}_s,\psi) = \int_{\Sigma} \rho_f \psi(\mathbf{u}_s\cdot\mathbf{n})\, d\Sigma, \tag{3}$$

the coupled eigenproblem is to find $(\omega,\mathbf{u}_s,\varphi)\in\mathbb{R}\times\mathcal{C}_s\times\mathcal{C}_f$ so that

$$\left\{\begin{array}{lcl} \forall \mathbf{v}\in\mathcal{C}_s, \quad \mathcal{K}_s(\mathbf{u}_s,\mathbf{v}) &=& \omega^2\mathcal{M}_s(\mathbf{u}_s,\mathbf{v}) + \omega^2\mathcal{C}_{fs}(\mathbf{v},\varphi), \\ \forall \psi\in\mathcal{C}_f, \quad 0 &=& \mathcal{M}_f(\varphi,\psi) - \mathcal{C}_{fs}(\mathbf{u}_s,\psi). \end{array}\right. \tag{4}$$

where $\mathcal{C}_s$ and $\mathcal{C}_f$ are the Hilbert spaces of kinematically admissible solid displacement and fluid potential fields:

$$\begin{array}{rcl} \mathcal{C}_s &=& \left\{\mathbf{v}\in H^1(\Omega_s) \text{ such that } \mathbf{v}=0 \text{ on } \Gamma_m\right\}, \\ \mathcal{F}_s &=& \left\{\psi\in H^1(\Omega_f) \text{ such that } \psi=0 \text{ on } \Gamma_l\right\}. \end{array} \tag{5}$$

These spaces are approached by the finite element spaces $\mathcal{C}_s^h$ and $\mathcal{C}_f^h$: quadratic functions for the solid displacement ($\mathbb{P}_2$, see Sec. 2.2), and linear functions for the fluid potential ($\mathbb{P}_1$), leading to the discretized matrix formulation linking the vectors of solid and fluid degrees of freedom:

$$\begin{pmatrix} \mathbb{K}_s & 0 \\ -\mathbb{C}_{fs}^T & \mathbb{M}_f \end{pmatrix} \begin{pmatrix} \mathbf{u}_s \\ \varphi \end{pmatrix} = \omega^2 \begin{pmatrix} \mathbb{M}_s & \mathbb{C}_{fs} \\ 0 & 0 \end{pmatrix} \begin{pmatrix} \mathbf{u}_s \\ \varphi \end{pmatrix} \tag{6}$$

While the pressure is prescribed on some subpart of the fluid boundary, the fluid mass matrix $\mathbb{M}_f$ can be inverted, and the fluid potential dofs can be eliminated through a Schur complement method ($\varphi = \mathbb{M}_f^{-1}\mathbb{C}_{fs}^T\mathbf{u}_s$), introducing an added-mass matrix $\mathbb{M}_a$ taking into account the influence of the motion of the water onto the vibrations of the latex membrane. The modal analysis of the non inflated membrane consists in the generalized eigenproblem:

$$\text{Find } (\omega,\mathbf{u}_s)\in\mathbb{R}\times\mathcal{C}_s^h \quad \text{such as} \quad \mathbb{K}_s\mathbf{u}_s = \omega^2\left(\mathbb{M}_s+\mathbb{M}_a\right)\mathbf{u}_s \quad \text{with} \quad \mathbb{M}_a = \mathbb{C}_{fs}\mathbb{M}_f^{-1}\mathbb{C}_{fs}^T \tag{7}$$

and is to be compared with the purely elastic problem where $\mathbb{M}_a$ is neglected.

2.2 Numerical results

Simulations have been conducted using the FreeFem++ software [8]. Default configuration considers a latex half-cylinder with inner radius $R = 10mm$, thickness $e = 0.25mm$ and length $L = 4.5cm$, density $\rho_s = 956kg/m^3$, Young modulus $E = 1.8MPa$ and Poisson's ratio $\nu = 0.49$.

A first two-dimensional purely elastic study has helped to define convergence with respect to meshing the solid domain. A structured mesh of Ω_s with 3 layers within the thickness (and circumference subdivision ensuring adequate mesh quality) is sufficient for functions in $\mathbb{P}_2$ while $\mathbb{P}_1$ elements would require at least 9 layers to reach the same precision, dramatically increasing memory requirement and CPU time. We do know that plate or shell elements can overcome that problem, but the current work is intended to be used as a reference for model reduction.

Table 1 presents a summary of the first eigenfrequencies in several configurations. It is noticeable that the 2D simulations lead to eigenfrequencies smaller than the ones resulting from the 3D computations. In fact, the 2D case refers to the displacement invariant relative to the axis of the cylinder, which is a configuration that is less stiff than the 3D case where Dirichlet boundaries conditions at the ends of the cylinder are imposed (which compares with the experimental setup).

Numerical experiments show that the mesh of the fluid domain does not need to conform to the solid mesh on the interface Σ (see also Ref. [7]) and that $\mathbb{P}_1$ basis functions are sufficient, with bigger elements size far from the inlet Γ_l and from the interface Σ. As visible in Table 1, the fluid motion clearly influences the behavior by strongly lowering the eigenfrequencies.

Table 1: Eigenfrequencies (Hz) of several problems: purely elastic or hydro-elastic, 2D or 3D study, $\mathbb{P}_1$ or $\mathbb{P}_2$ basis functions. Default mesh for Ω_s is made of 3 layers

Case	1st mode	2nd mode	3rd mode	4th mode	5th mode	6th mode
Elastic 2D $\mathbb{P}_1$	38.4	84.0	155.9	238.0	344.5	457.7
Elastic 2D $\mathbb{P}_2$	24.6	54.0	100.1	153.3	221.5	296.3
Elastic 2D $\mathbb{P}_2$ with 10 layers	24.4	53.7	99.5	152.4	220.1	294.5
Elastic 3D $\mathbb{P}_2$	97.7	104.5	157.1	164.5	165.4	166.1
Hydro-elastic 2D solid $\mathbb{P}_2$ - fluid $\mathbb{P}_1$	8.8	21.8	45.5	64.5	78.7	121.1

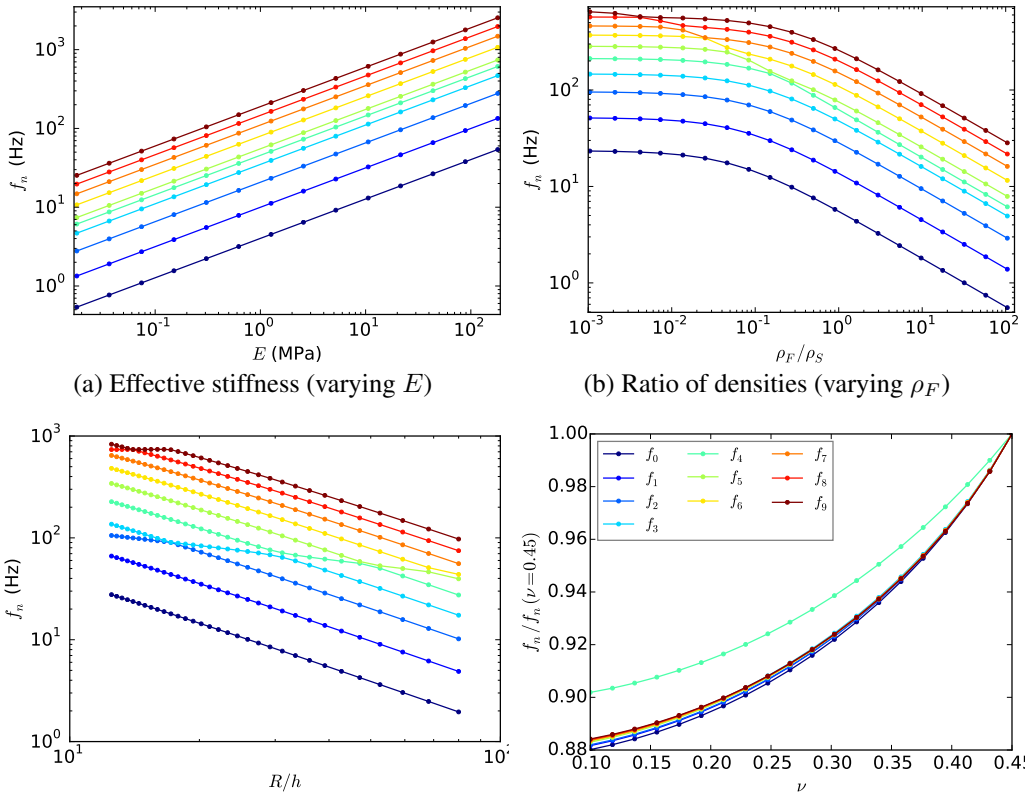

(a) Effective stiffness (varying E)

(b) Ratio of densities (varying ρ_F)

(c) Aspect ratio (varying h)

(d) Poisson's ratio (varying ν)

Figure 2: Influence of the four dimensionless quantities on the eigenfrequencies.

A parametric study of a similar hydro-elastic coupling evidenced (see Ref. [6]) four dimensionless quantities while normalizing with the radius R of the cylinder, the thickness e of the latex and some arbitrary frequency Ω: the aspect ratio e/R, the ratio of densities ρ_s/ρ_f, the Poisson's ratio ν and the effective stiffness of the membrane $K_{\text{eff}} = E/(\rho_s R^2\Omega^2)$. Figure 2 highlights this dependence: while the stiffness and the low aspect ratio seems to act as a mere multiplicative factor, the influence of the ratio of densities enhances the difference between light and heavy fluid loading. Figures 2b-2d also evidence that there is at least one eigenfrequency with a variation that differs from the others (f_4 in Fig. 2d, it crosses the others frequencies in the other plots). Investigating the eigenvectors, it appears that almost all the modes correspond to hydro-elastic motions with an effective coupling, while the singular mode (others singular modes appear at higher frequencies) correspond to modes essentially

localized at the pressure inlet, i.e. with little participation of the membrane, as visible in Fig. 3. As performed in Ref [6], it is possible to discriminate the kind of modes by comparing the fluid and solid kinetic energy of the modal shapes (preferably when normalized with respect to the total mass matrix).

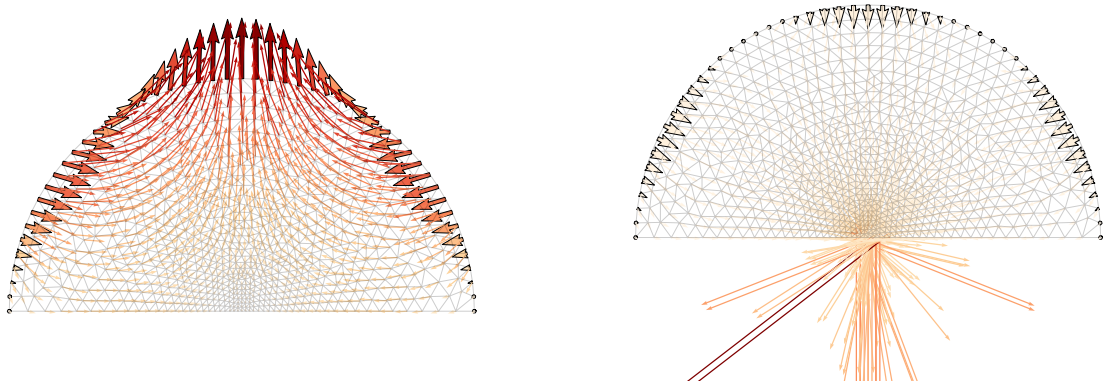

(a) Mode 2 (b) Mode 5

Figure 3: Modal shapes highlighting vibration localization at the pressure inlet for mode 5. Scaling is identical for solid and fluid displacements.

3. Analysis of the inflated membrane

While predicting the influence of the fluid loading on the vibrations of the latex membrane, the linear modeling presented in the previous section does not account for the effect of the static pressure in the water. As this is a primary control parameter of the replicas used to simulate the phonation, it is essential to be able to predict how the pressure controls the mechanical resonances. The modeling is hereafter adapted to take into account the prestress coming from the static inflation, and a modal analysis of the inflated state is then performed. We will consider the initial configuration Ω_0, the configuration after inflation Ω_S , and the inflated-deformed configuration Ω_*, as well as the respective transformations φ_S and φ_*.

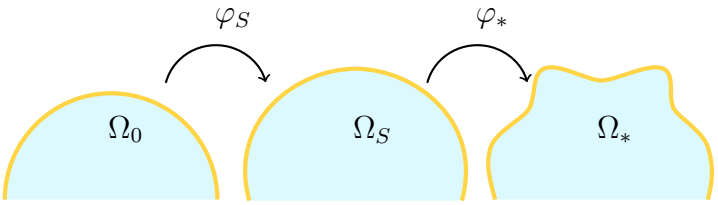

3.1 Static equilibrium configuration

Water pressure p (up to $10\,kPa$) can induce moderate to large displacements and requires a Lagrangian formulation of the problem on the Ω_0 configuration, with the introduction of the deformation gradient tensor $\mathbf{F}(\mathbf{u}_s)$, its determinant $J(\mathbf{u}_s)$, the Green-Lagrange tensor $\mathbf{E}(\mathbf{u}_s)$ and the 1^{st} and 2^{nd} Piola- Kirchhoff tensors $\Pi(\mathbf{u}_s)$ and $\mathbf{S}(\mathbf{u}_s)$:

$$\mathbf{F}(\mathbf{u}_s) = \mathbf{I} + \nabla_X \mathbf{u}_s, \quad \mathbf{E}(\mathbf{u}_s) = 1/2\,(\mathbf{F}(\mathbf{u}_s)^T \cdot \mathbf{F}(\mathbf{u}_s) - \mathbf{I}), \quad \text{and} \quad \Pi(\mathbf{u}_s) = \mathbf{F}(\mathbf{u}_s) \cdot \mathbf{S}(\mathbf{u}_s). \tag{8}$$

For the sake of simplicity, we assume *a priori* a St Venant-Kirchhoff constitutive law, a hyper-elastic extension of isotropic linear elastic model:

$$\mathbf{S}(\mathbf{u}_s) = \mathcal{C} : \mathbf{E}(\mathbf{u}_s) = \lambda\ \mathrm{tr}(\mathbf{E}(\mathbf{u}_s))\,\mathbf{I} + 2\mu\mathbf{E}(\mathbf{u}_s). \tag{9}$$

Neglecting volume forces and traction on the Γ_{ext} boundary, the variational formulation writes, on the initial undeformed configuration:

$$\forall\, \mathbf{v} \in \mathcal{C}_s, \int_{\Omega_0} \mathbf{S}(\mathbf{u}_s) : \left(\left.\frac{\partial \mathbf{E}}{\partial \mathbf{u}}\right|_{\mathbf{u}_s} \cdot \mathbf{v} \right) - \int_{\Sigma_0} pJ(\mathbf{u}_s)(\mathbf{F}(\mathbf{u}_s)^{-T} \cdot \mathbf{N}) \cdot \mathbf{v} = 0 \tag{10}$$

with the Lagrangian gradient operator ∇_X. The left hand side is denoted $R(\mathbf{u}_s, \mathbf{v})$ and its first term $\mathcal{K}_{\text{NL}}(\mathbf{u}_s, \mathbf{v})$ generalizes the linear stiffness operator $\mathcal{K}_s$ in the finite strain framework. The second term is a follower pressure term denoted $f_{\text{NL}}(\mathbf{u}_s, \mathbf{v})$ that accounts for the variation (in size and orientation) of the surface the water pressure applies on. The problem appears now as non-linear due to both the two contributions. The zero of the nonlinear operator R is searched using a modified Newton procedure. The non-symmetric contribution of f_{NL} to the tangent matrix is ignored, the approximation of the tangent matrix being non critical with respect to the convergence of the Newton scheme. At each iteration k, we then look for the increment $\mathbf{w}$ solving the linear system:

$$\forall\, \mathbf{v},\ R(\mathbf{u}_s^k, \mathbf{v}) + \left.\frac{\partial K_{\text{NL}}}{\partial \mathbf{u}}\right|_{\mathbf{u}_s^k, \mathbf{v}} \cdot \mathbf{w} = 0 \quad \text{then} \quad \mathbf{u}_s^{k+1} = \mathbf{u}_s^k + \mathbf{w}. \tag{11}$$

with a convergence criterion of 10^{-7} using the $\mathcal{L}_2$-norm of $\mathbf{w}$ relative to the one of the iterated $\mathbf{u}_s^k$. The expanded expressions of Eq. (11) can be found in Ref. [9].

The vector field $\mathbf{u}_0$ solution of Eq. (10) is then used to calculate $J(\mathbf{u}_0)$, $\mathbf{E}(\mathbf{u}_0)$ and $\mathbf{S}(\mathbf{u}_0)$. We finally deduce the Cauchy stress in the inflated configuration by the expression:

$$\sigma_0 = \sigma(\mathbf{u}_0) = J(\mathbf{u}_0)^{-1} \mathbf{F}(\mathbf{u}_0) \cdot \mathbf{S}(\mathbf{u}_0) \cdot \mathbf{F}(\mathbf{u}_0)^T. \tag{12}$$

Fig. 4 compares the maximal transverse displacement on the centerline of the replica. The experimental data are extracted from the detection of the glottal contours on pictures taken for various water pressure. Taking into account the nonlinear behavior of the material improves the prediction of the static inflation of the replica in comparison with the small strain inflation model. Linear elasticity greatly overestimates the inflation, while the finite strain theory leads to slightly underestimated values. This computation also enables to evaluate the range of strain to consider. Up to a water pressure of $10kPa$, strain remains at most of 10%, justifying *a posteriori* the choice of the St Venant-Kirchhoff behavior law instead of more commonly used ones, e.g. Mooney-Rivlin or Ogden models.

3.2 Modal analysis with prestress

In the manner of Ref. [5], the introduction of small vibrations $\mathbf{u}_*$ in the vicinity of the static inflated configuration results in the eigenproblem:

$$\text{Find } (\omega, \mathbf{u}_*) \in \mathbb{R} \times \mathcal{C}_s^h \quad \text{such as} \quad \forall \mathbf{v} \in \mathcal{C}_s,\ \left.\frac{\partial R}{\partial \mathbf{u}}\right|_{\mathbf{u}_0, \mathbf{v}} \cdot \mathbf{u}_* = \omega^2 \left(\mathcal{M}_s + \mathcal{M}_a\right)(\mathbf{u}_*, \mathbf{v}) \tag{13}$$

where the tangent stiffness operator replaces the previous linear elastic stiffness operator. It can be obtained as the last tangent operator of the modified Newton procedure described in Sec. 3.1. It is worth to provide some insight on its components. First the gradient of the nonlinear stiffness operator $\mathcal{K}_{\text{NL}}$ writes:

$$\left.\frac{\partial \mathcal{K}_{\text{NL}}}{\partial \mathbf{u}}\right|_{\mathbf{u}_0, \mathbf{v}} \cdot \mathbf{u}_* = \int_{\Omega_0} \left(\left.\frac{\partial \mathbf{E}}{\partial \mathbf{u}}\right|_{\mathbf{u}_0} \cdot \mathbf{u}_* \right) : \mathcal{C} : \left(\left.\frac{\partial \mathbf{E}}{\partial \mathbf{u}}\right|_{\mathbf{u}_0} \cdot \mathbf{v} \right) + \mathbf{S}(\mathbf{u}_0) : (\nabla_X \mathbf{u}_* \cdot \nabla_X \mathbf{v}). \tag{14}$$

The first term describes the stiffening/softening effect of the initial deformation of the structure (*pre-deformation* stiffness operator) while the second one is the so-called *geometric* stiffness operator

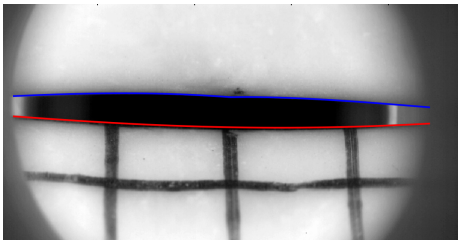

(a) $P = 5kPa$

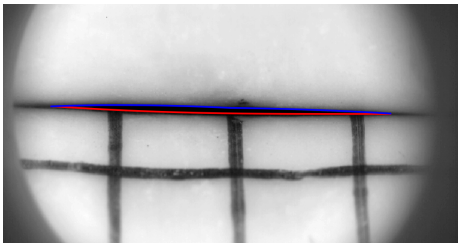

(b) $P = 11.5kPa$

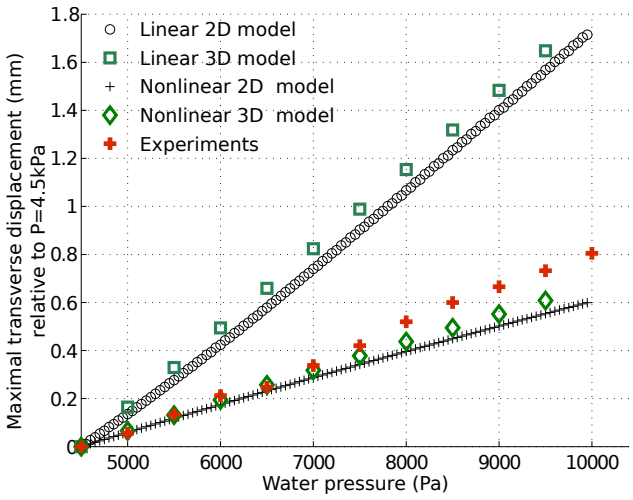

(c) Comparison of 2D vs 3D and linear vs nonlinear models.

Figure 4: Static maximal normal displacement of latex under water pressure P_{water}

related to the initial stresses $\mathbf{S}(\mathbf{u}_0)$. In addition, contrary to the hydro-elastic linear model, the follower pressure should contribute too for the tangent stiffness operator, but it is ignored in the present study.

Last it should be emphasized that the fluid is supposed to be at rest under pressure p in the inflated configuration, i.e. the inflation is supposed to have little influence on the fluid configuration. However the added-mass operator should be evaluated taking into account the inflated geometry: the coupling $\mathcal{C}_{fs}$ and the fluid mass $\mathcal{M}_f$ operators involve integration on the deformed interface and deformed fluid domain, respectively.

In conclusion, the water pressure influences the modal analysis through several means:

– the stiffness operator corresponds now to the tangent stiffness operator evaluated in the inflated configuration,

– the added-mass operator that accounts for the effect of the fluid load on the structure vibration now also depends on the deformed geometry, which in turns results from the water pressure.

Fig. 5 presents the variation of the first eigenfrequency depending on the water pressure, for several values of the Poisson's ratio and of the thickness of the latex membrane. The theory predicts the increase of the frequency for low inflation but a decrease appears above a threshold that depends on the geometric and mechanical characteristics of the structure. This is in contradiction with the experiments which does not exhibit the non-monotonic evolution. Several hypothesis are under investigation, among which the bad conditioning of the displacement based formulation. Ref. [9] mentions that displacement-pressure formulations may behave better when approaching the incompressible limit $\nu = 0.5$.

4. Conclusion

A linear hydro-elastic model has first been presented, showing interesting features in terms of kinds of modes that can exist in the fluid-structure interaction under study. Considering its failure in retrieving the experimentally observed behavior, i.e. the influence of the water pressure on the eigenfrequencies, it has been extended to include the effect of the pressure in terms of static inflation and of pressure-dependent eigenmodes, by means of the tangent stiffness operator accounting for the pre-stress and for the pre-deformation. The first results evidence the ability to predict this dependency, but also show some limitations that may be due to the known bad performance of the displacement based formulation near the incompressible limit behavior. It was also computed in the static study

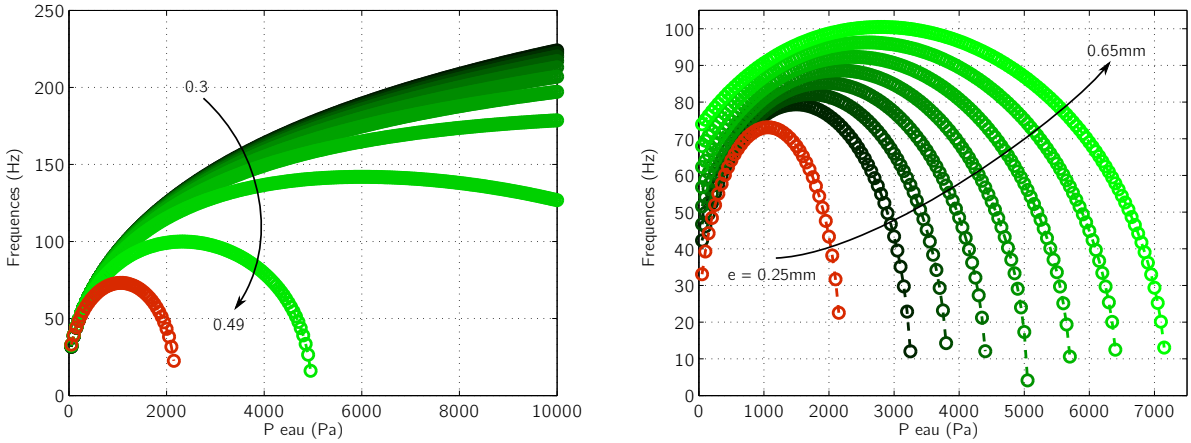

(a) (b)

Figure 5: Evolution of the first eigenfrequency with the water pressure for various values of the Poisson's ratio (a) or of the latex thickness (b).
The red curves show the default configuration: $\nu = 0.49$ and $e = 0.25mm$.

that moderate strain occurs in the latex in the range of experimental water pressure, thus justifying the use of a moderately hyper elastic law such as the St Venant-Kirchhoff one.

Acknowledgments

This work was partially supported by grant VoFoCam (ANR-12-PDOC-0018) of the ANR french funding agency.

REFERENCES

1. Berg, J.v.d., Zantema, J.T. and P. Doornenbal, J., On the air resistance and the bernoulli effect of the human larynx, *J. Acous. Soc. Am.*, **29** (5), 626–631 (1957).

2. Ruty, N., Pelorson, X., Hirtum, A.V., Lopez-Arteaga, I. and Hirschberg, A., An in vitro setup to test the relevance and the accuracy of low-order vocal folds models, *J. Acous. Soc. Am.*, **121** (1), 479–490 (2007).

3. Pelorson, X. and Laval, X., An experimental replica of the vocal folds to study normal and pathological voice, *12th CFA*, Nantes, France (2012).

4. Rajan, A. and Kochupillai, J., Dynamic analysis of a pressure prestressed in vacuo torus with follower load stiffness, *Proc. Inst. Mech. Eng., Part C: J. Mech. Eng. Sc.* (2014).

5. Schotté, J.S. and Ohayon, R., Various modelling levels to represent internal liquid behaviour in the vibration analysis of complex structures, *Comp. Meth. Appl. Mech. Eng.*, **198** (21–26), 1913–1925 (2009).

6. Hermant, N., *Observation, modélisation et simulation des vibrations des maquettes de plis vocaux. Applications à des configurations pathologiques*, Ph.D. thesis, Univ. Grenoble (2014).

7. Bermúdez, A., Rodríguez, R and Santamarina, D., A finite element solution of an added mass formulation for coupled fluid-solid vibrations, *Num. Math.*, **87** (2), 201–227 (2000).

8. Hecht, F., New development in freefem++, *J. Numer. Math.*, **20** (3-4), 251–265 (2012).

9. Fortin, A. and Garon, A., Les éléments finis: de la théorie à la pratique, Univ. Laval, Canada (2011). `http://www.giref.ulaval.ca/~afortin/cours_elements_finis/documents/notes_elements_finis.pdf` (last viewed 03/13/2015).